Int J Theor Phys (2010) 49: 2364–2378
DOI 10.1007/s10773-010-0423-1

Thin-Shell Wormholes from Regular Charged Black Holes

F. Rahaman · K.A. Rahman · S.A. Rakib · Peter K.F. Kuhfittig

Received: 26 April 2010 / Accepted: 2 July 2010 / Published online: 22 July 2010

Abstract We investigate a new thin-shell wormhole constructed by surgically grafting two regular charged black holes arising from the action using nonlinear electrodynamics coupled to general relativity. The stress-energy components within the shell violate the null and weak energy conditions but obey the strong energy condition. Several other aspects of this thin-shell wormhole are also analyzed. The most important finding is that the presence of a charge is essential for producing a thin-shell wormhole that is stable to linearized spherically symmetric perturbations about a static equilibrium solution. The precise conditions depend on various properties of the black hole.

Keywords Thin-shell wormholes · Nonlinear electrodynamics · Regular black holes

1 Introduction

Over 20 years ago Visser [1] proposed a theoretical method for constructing a new class of wormholes from a black-hole spacetime. This type of wormhole is known as a thin-shell wormhole and is constructed by applying the so-called cut-and-paste technique: surgically graft two black-hole spacetimes together in such a way that no event horizon is permitted to form. This method yields a wormhole spacetime whose throat is a time-like hypersurface, i.e., a three-dimensional thin shell. Since Visser's novel approach yields a way of minimizing the use of exotic matter to construct a wormhole, the technique was quickly adopted by various authors for constructing thin-shell wormholes [2–20].

In 1999, E. Ayon-Beato and A. García [21] discovered a new regular exact black hole solution which comes from the action using nonlinear electrodynamics coupled to general

F. Rahaman (✉) · K.A. Rahman · S.A. Rakib
Department of Mathematics, Jadavpur University, Kolkata 700 032, West Bengal, India
e-mail: farook_rahaman@yahoo.com

P.K.F. Kuhfittig
Department of Mathematics, Milwaukee School of Engineering, Milwaukee, WI 53202-3109, USA
e-mail: kuhfitti@msoe.edu

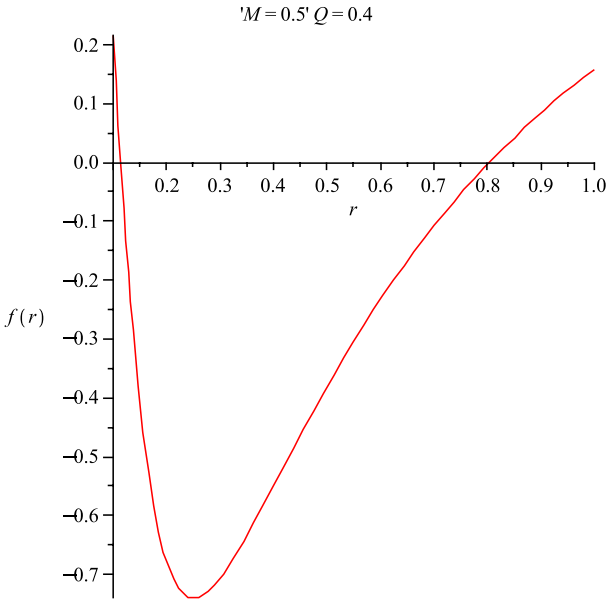

Fig. 1 Event horizons occur at r_- and r_+, where $f(r)$ cuts the r-axis, using suitable parameters. Here $M = 0.5$ and $Q = 0.4$

relativity. The dynamics of the theory is governed by the action

$$I = \frac{1}{16\pi}\int d^4x\,\sqrt{-g}\big[R - L(F)\big]. \tag{1}$$

Here the nonlinear electrodynamics is described by a type of gauge-invariant Lagrangian $L(F)$, where $F_{\mu\nu}$ is the Maxwell field tensor, F is the contracted Maxwell scalar, i.e., $F^{\mu}_{\mu} = F$, while R is the curvature scalar. According to Ref. [21], while there are more general Lagrangians, the form of the action in (1) is sufficient for present purposes.

To obtain the desired solution from the above action (1), Ayon-Beato and García considered a static and spherically symmetric configuration given by

$$ds^2 = -f(r)\,dt^2 + f(r)^{-1}\,dr^2 + r^2\big(d\theta^2 + \sin^2\theta\,d\phi^2\big), \tag{2}$$

where

$$f(r) = 1 - \frac{2M}{r} + \frac{2M}{r}\tanh\left(\frac{Q^2}{2Mr}\right). \tag{3}$$

Here the parameters M and Q can be associated with mass and charge, respectively, of the black hole.

It is shown in Ref. [21] that this black hole has two event horizons r_- and r_+ whenever $|Q| < 1.05M$. So for suitable choices of the parameters M and Q, the points r_- and r_+ are simply the r-intercepts of $f(r)$ (see Fig. 1).

In this paper we employ such a class of regular charged black holes by starting with two copies thereof and constructing a traversable thin-shell wormhole by means of the cut-and-paste technique, as described in Sect. 2. It is shown that at the junction surface the null and weak energy conditions are violated. The total amount of exotic matter required is also discussed.

Our final and most important topic is the question of stability to a linearized spherically symmetric perturbation. The analysis is carried out with the help of a parameter β, which is usually interpreted as the speed of sound, implying that $0 < \beta^2 \leq 1$. These values of β correspond to a single region of stability for a fairly narrow range of values of M, Q, and the radius of the junction surface. The reason for starting with two regular charged black holes can be seen from the following: If $Q = 0$, that is, if the two spacetimes are Schwarzschild, then the wormholes are unstable for all values of the radii whenever $0 < \beta^2 \leq 1$ [2]. So the presence of a charge Q is essential to the stability of the thin-shell wormhole. As expected, the other properties of the regular charged black hole, such as the metric (2), and the condition $|Q| < 1.05M$ come into play as well.

2 Thin-shell wormhole construction

The mathematical construction of our thin-shell wormhole begins by taking two copies of the regular charged black hole and removing from each the four-dimensional region

$$\Omega^{\pm} = \{r \leq a \mid a > r_h\}.$$

Here $r_h = r_+$, the larger of the two radii. We now identify (in the sense of topology) the timelike hypersurfaces

$$\partial\Omega^{\pm} = \{r = a \mid a > r_h\},$$

denoted by Σ. The resulting manifold is geodesically complete and consists of two asymptotically flat regions connected by a throat. The induced metric on Σ is given by

$$ds^2 = -d\tau^2 + a(\tau)^2\big(d\theta^2 + \sin^2\theta\, d\phi^2\big), \tag{4}$$

where τ is the proper time on the junction surface. Using the Lanczos equations [1–20],

$$S^i{}_j = -\frac{1}{8\pi}\big([K^i{}_j] - \delta^i{}_j[K]\big),$$

one can obtain the surface stress-energy tensor $S^i{}_j = \mathrm{diag}(-\sigma, p_\theta, p_\phi)$, where σ is the surface-energy density and $p = p_\theta = p_\phi$ is the surface pressure. The Lanczos equations now yield

$$\sigma = -\frac{1}{4\pi}\big[K^\theta{}_\theta\big]$$

and

$$p = \frac{1}{8\pi}\big([K^\tau{}_\tau] + [K^\theta{}_\theta]\big).$$

A dynamic analysis can be obtained by letting the radius $r = a$ be a function of time [2]. As a result,

$$\sigma = -\frac{1}{2\pi a}\sqrt{f(a) + \dot{a}^2} \tag{5}$$

and

$$p_\theta = p_\phi = p = -\frac{1}{2}\sigma + \frac{1}{8\pi}\frac{2\ddot{a} + f'(a)}{\sqrt{f(a)+\dot{a}^2}}. \tag{6}$$

Here p and σ obey the conservation equation

$$\frac{d}{d\tau}\left(\sigma a^2\right) + p\frac{d}{d\tau}(a^2) = 0 \tag{7}$$

or

$$\dot{\sigma} + 2\frac{\dot{a}}{a}(p+\sigma) = 0. \tag{8}$$

In the above equations, the overdot and prime denote, respectively, the derivatives with respect to τ and a.

For a static configuration of radius a, we obtain (assuming $\dot{a} = 0$ and $\ddot{a} = 0$) from (5) and (6)

$$\sigma = -\frac{1}{2\pi a}\left[1 - \frac{2M}{a} + \frac{2M}{a}\tanh\left(\frac{Q^2}{2Ma}\right)\right]^{\frac{1}{2}} \tag{9}$$

and

$$p = \frac{[1 - \frac{M}{a} + \frac{M}{a}\tanh(\frac{Q^2}{2Ma}) - \frac{Q^2}{2a^2}\cosh^{-2}(\frac{Q^2}{2Ma})]}{4\pi a[1 - \frac{2M}{a} + \frac{2M}{a}\tanh(\frac{Q^2}{2Ma})]^{\frac{1}{2}}}. \tag{10}$$

Observe that the energy-density σ is negative. Moreover, on this shell, which is infinitely thin, the radial pressure is zero. So the shell contains matter that violates both the null energy condition (NEC) and the weak energy condition (WEC). Also, since $\sigma + 2p$ and $\sigma + 3p$ are positive, the strong energy condition is satisfied.

Using various values of the parameters M and Q, Figs. 2–8 show the plots for σ and p as functions of the radius a. We choose typical wormholes whose radii fall within the range 0.01 to 10 km.

3 Equation of State

Let us suppose that the EoS at the surface Σ is $p = w\sigma$, $w \equiv$ constant. From (9) and (10),

$$\begin{aligned}\frac{p}{\sigma} &= w \\ &= -\frac{1}{2} - \frac{M}{2a}\frac{[1 - \tanh(\frac{Q^2}{2Ma}) - \frac{Q^2}{2Ma}\cosh^{-2}(\frac{Q^2}{2Ma})]}{4\pi a[1 - \frac{2M}{a} + \frac{2M}{a}\tanh(\frac{Q^2}{2Ma})]}.\end{aligned} \tag{11}$$

Observe that if $a \to \infty$, i.e., the location of the wormhole throat is large enough, then $w \to -\frac{1}{2}$. When $a \to a_0$, where a_0 is the point where the curve cuts the a-axis in Fig. 9, then $p \to 0$, which would normally be viewed as a dust shell. Since $a_0 < r_h$, however, the dust shell is never be found. On the other hand, since the Casimir effect with a massless field is of the traceless type, it may be of interest to check the traceless surface stress-energy tensor,

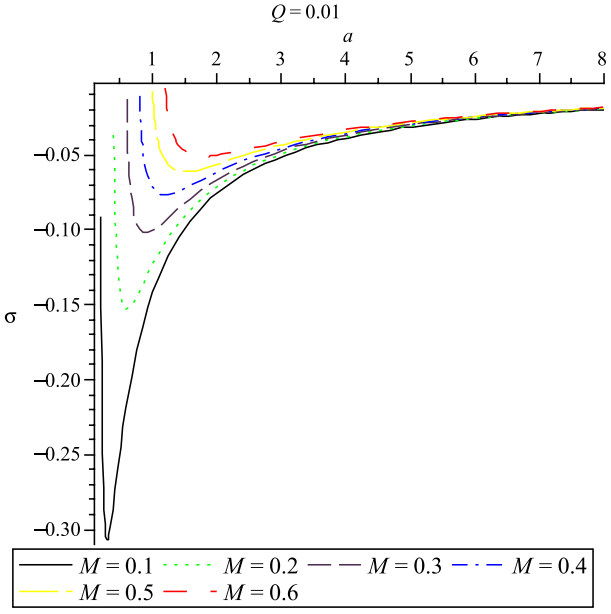

Fig. 2 Plots for σ versus a. We choose the fixed value $Q = 0.01$ and various values for M

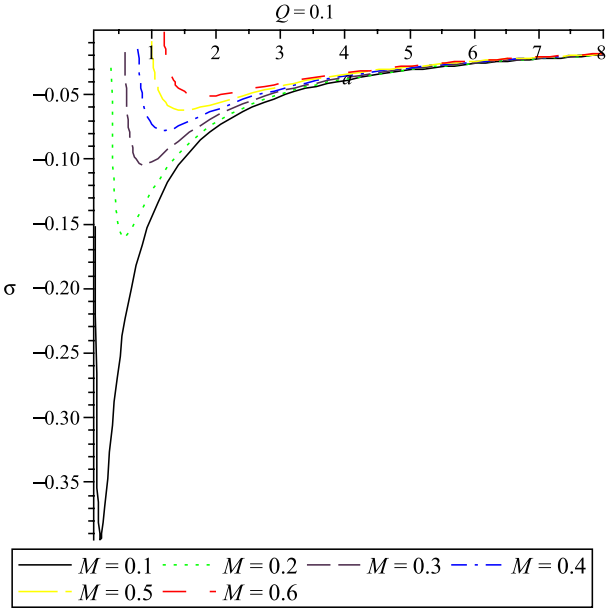

Fig. 3 Plots for σ versus a. We choose the fixed value $Q = 0.1$ and various values for M

$S^i{}_j = 0$, i.e., $-\sigma + 2p = 0$. From this equation we find that

$$g(a) \equiv 4 - \frac{6M}{a} + \frac{6M}{a}\tanh\left(\frac{Q^2}{2Ma}\right) - \frac{Q^2}{a^2}\cosh^{-2}\left(\frac{Q^2}{2Ma}\right) = 0. \tag{12}$$

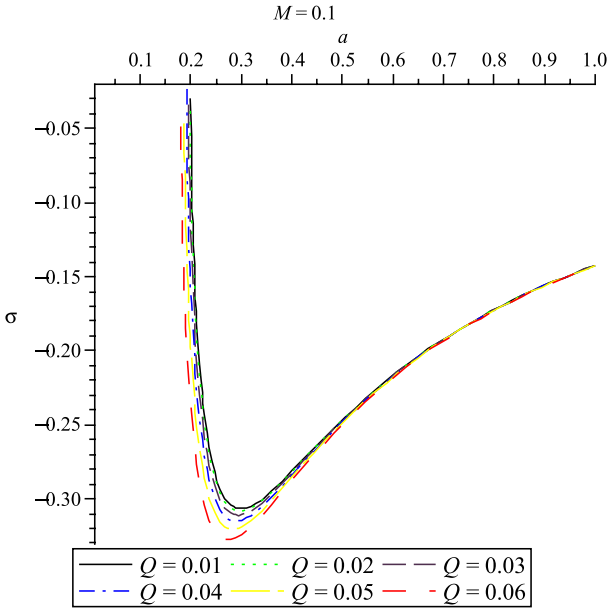

Fig. 4 Plots for σ versus a. We choose the fixed value $M = 0.1$ and various values for Q

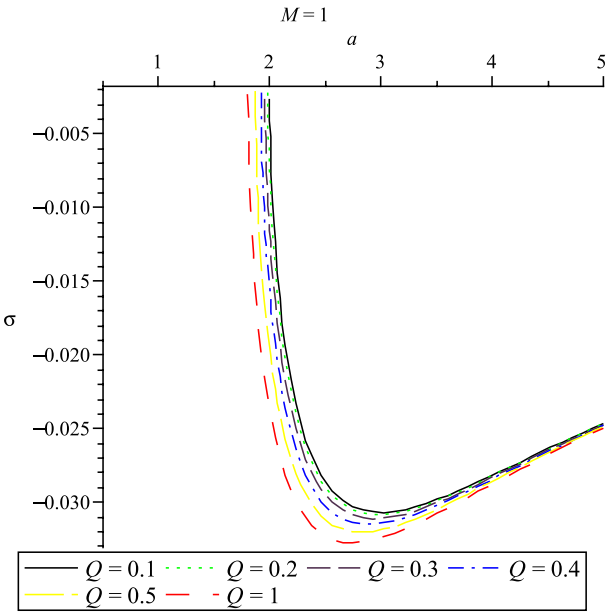

Fig. 5 Plots for σ versus a. We choose the fixed value $M = 1$ and various values for Q

Figure 10 indicates that the value of a satisfying this equation is inside the event horizon ($r = r_h$) of the regular black hole. It follows that this situation cannot arise in a wormhole setting.

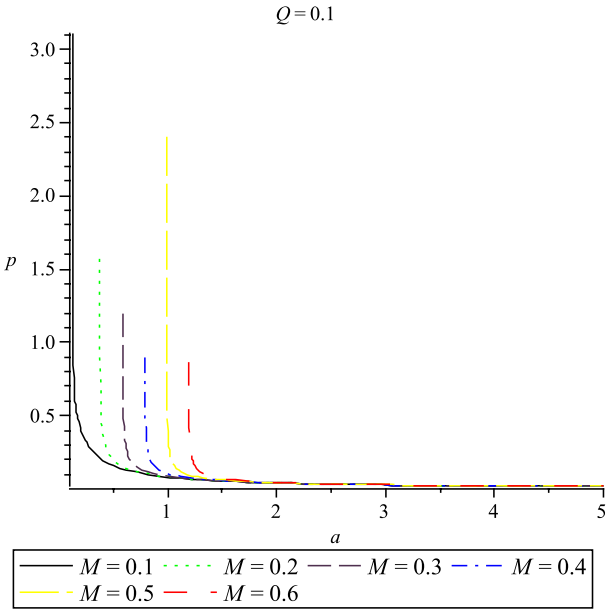

Fig. 6 Plots for p versus a. We choose the fixed value $Q = 0.1$ and various values for M

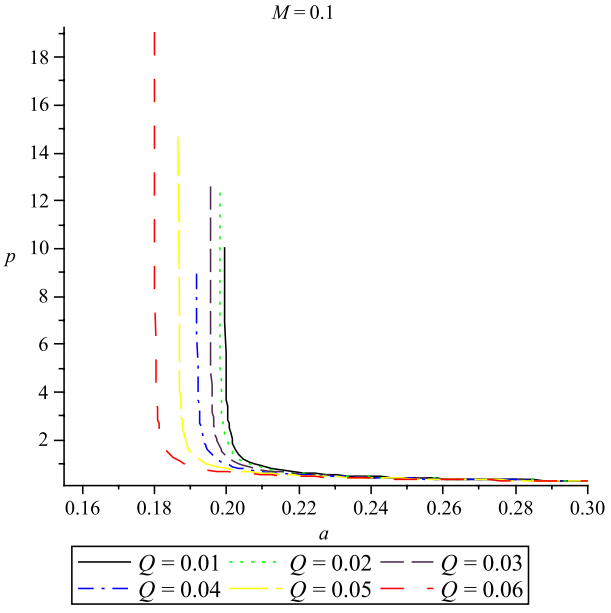

Fig. 7 Plots for p versus a. We choose the fixed value $M = 0.1$ and various values for Q.

4 The Gravitational Field

In this section we are going to take a brief look at the attractive or repulsive nature of our wormhole. To do so, we calculate the observer's four-acceleration

$$a^{\mu} = u^{\mu}_{;\nu} u^{\nu},$$

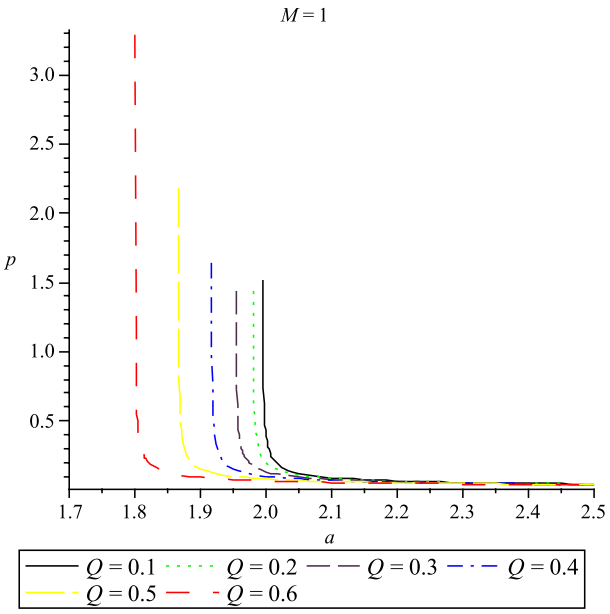

Fig. 8 Plots for p versus a. We choose the fixed value $M = 1$ and various values for Q

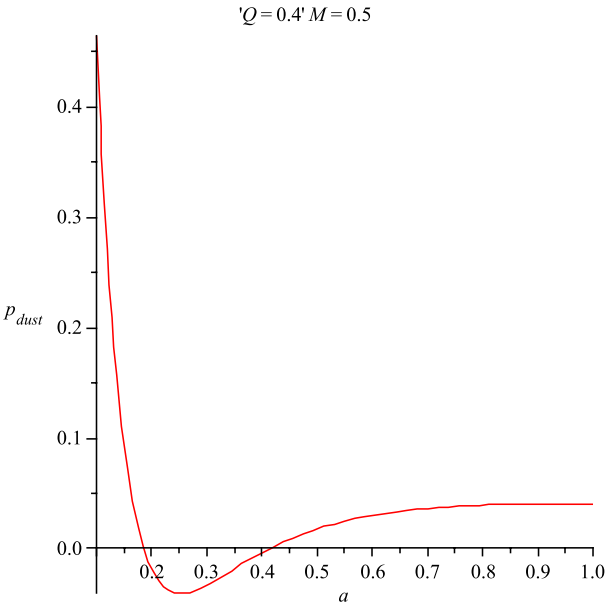

Fig. 9 The curve cuts the a-axis at $a_0 < r_h$; for the given plot, $M = 0.5$ and $Q = 0.4$

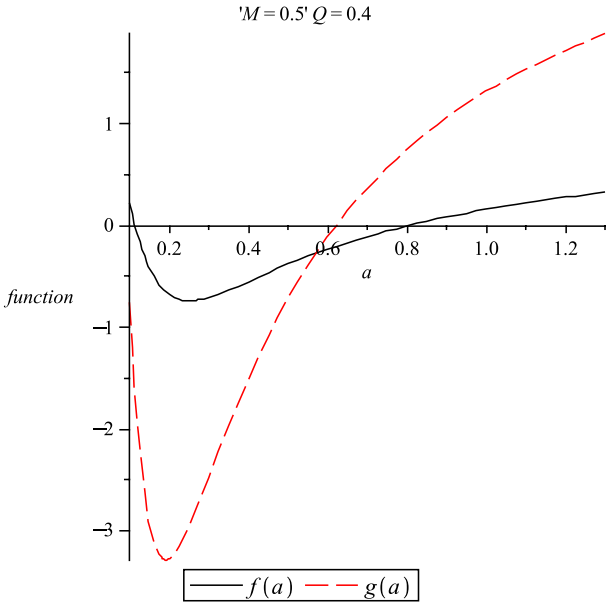

Fig. 10 The curve $g(a)$ cuts the a-axis at a point less than r_h; for the given plot, $M = 0.5$ and $Q = 0.4$

where

$$u^v = \frac{dx^v}{d\tau} = \left(\frac{1}{\sqrt{f(r)}}, 0, 0, 0\right).$$

Taking into account (2), the only nonzero component is given by

$$a^r = \Gamma^r_{tt}\left(\frac{dt}{d\tau}\right)^2 = \frac{M}{r^2}\alpha(r),$$

where

$$\alpha(r) = \left[1 - \tanh\left(\frac{Q^2}{2Mr}\right) - \frac{Q^2}{2Mr}\cosh^{-2}\left(\frac{Q^2}{2Mr}\right)\right]. \tag{13}$$

A test particle moving radially from rest obeys the geodesic equation

$$\frac{d^2r}{d\tau^2} = -\Gamma^r_{tt}\left(\frac{dt}{d\tau}\right)^2 = -a^r.$$

It is true in general that a wormhole is attractive whenever $a^r > 0$. In our situation, a^r is positive for $r > \frac{Q^2}{2Mr_0}$, where r_0 is the point where $\alpha(r)$ cuts the x-axis in Fig. 11. In other words, the wormhole is attractive for $r > \frac{Q^2}{2Mr_0}$ and repulsive for $r < \frac{Q^2}{2Mr_0}$. Finally, an observer at rest is a geodesic observer whenever $r = \frac{Q^2}{2Mr_0}$.

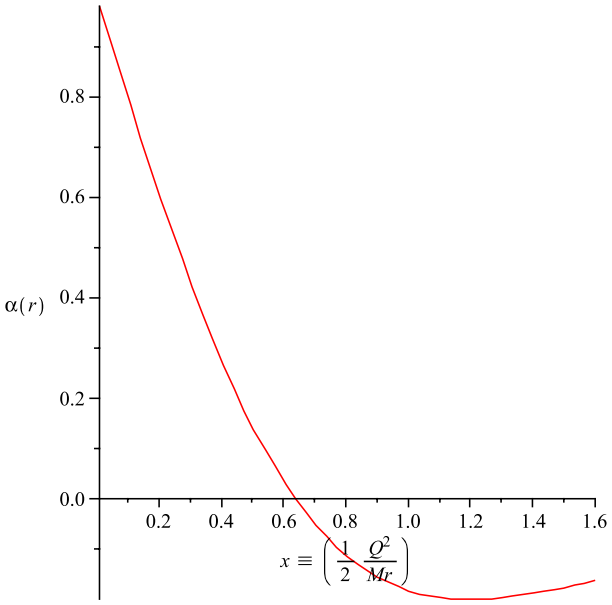

Fig. 11 r_0 is the point where $\alpha(r)$ cuts the x-axis

5 The Total Amount of Exotic Matter

In this section we determine the total amount of exotic matter for the thin-shell wormhole. This total can be quantified by the integral [7–13]

$$\Omega_\sigma = \int [\rho + p]\sqrt{-g}\, d^3x. \tag{14}$$

By introducing the radial coordinate $R = r - a$, we get

$$\Omega_\sigma = \int_0^{2\pi}\int_0^{\pi}\int_{-\infty}^{\infty} [\rho + p]\sqrt{-g}\, dR\, d\theta\, d\phi.$$

Since the shell is infinitely thin, it does not exert any radial pressure. Moreover, $\rho = \delta(R)\sigma(a)$. So

$$\begin{aligned}\Omega_\sigma &= \int_0^{2\pi}\int_0^{\pi} [\rho\sqrt{-g}]|_{r=a} d\theta\, d\phi = 4\pi a^2\sigma(a)\\ &= 4\pi a^2\left(-\frac{1}{2\pi a}\right)\sqrt{1 - \frac{2M}{a} + \frac{2M}{a}\tanh\left(\frac{Q^2}{2Ma}\right)}\\ &= -2a\sqrt{1 - \frac{2M}{a} + \frac{2M}{a}\tanh\left(\frac{Q^2}{2Ma}\right)}.\end{aligned} \tag{15}$$

This NEC violating matter (Ω_σ) can be reduced by choosing a value for a closer to $r = r_h$. The closer a is to r_h, however, the closer the wormhole is to a black hole: incoming microwave background radiation would get blueshifted to an extremely high temperature [22]. On the other hand, it follows from (15) that for $a \gg r_h$, Ω_σ will depend linearly

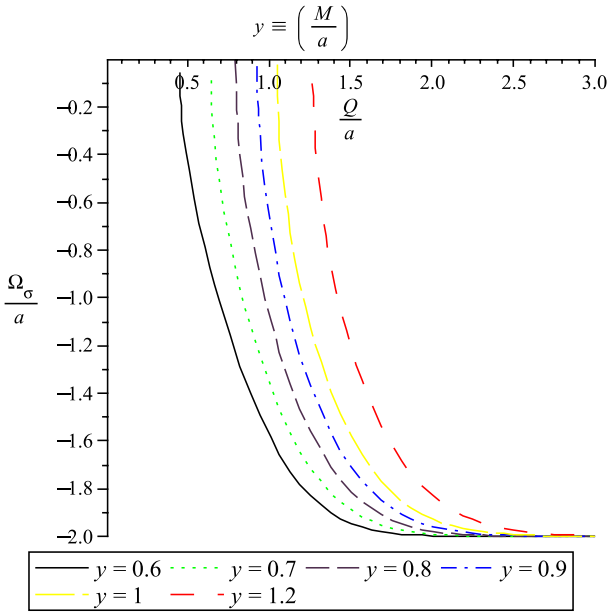

Fig. 12 The variation in the total amount of exotic matter on the shell with respect to the charge of the black hole, while assuming a fixed mass for the black hole

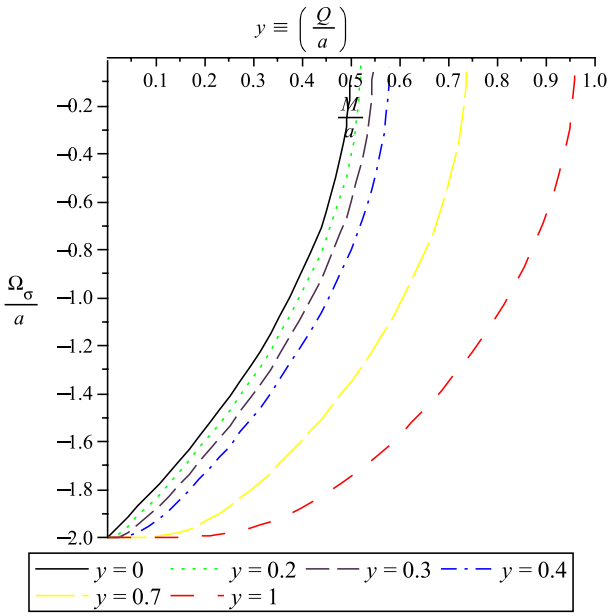

Fig. 13 The variation in the total amount of exotic matter on the shell with respect to the mass of the black hole, while assuming a fixed charge for the black hole

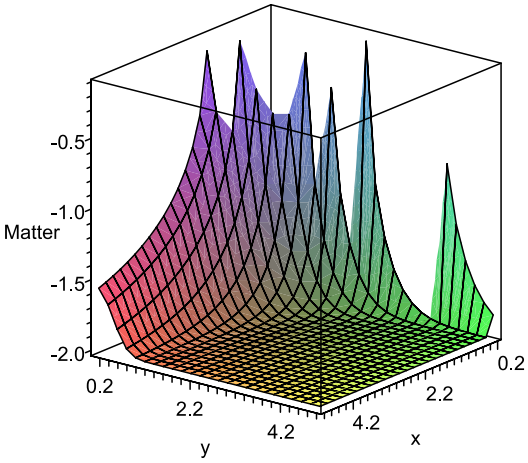

Fig. 14 The variation in the total amount of exotic matter on the shell with respect to the mass ($x = \frac{M}{a}$) and the charge ($y = \frac{Q}{a}$) of the black hole

on a:

$$\Omega_\sigma \approx -2a. \tag{16}$$

The variation of the total amount of exotic matter with respect to the mass and charge of the black hole can best be seen graphically (Figs. 12–14). Observe that the mass on the thin shell can be reduced by either increasing the mass or decreasing the charge of the black hole.

6 Linearized Stability

In this section we will focus our attention on the stability of the configuration under small perturbations around a static solution at $a = a_0$.

Rearranging (5), we obtain the thin shell's equation of motion

$$\dot{a}^2 + V(a) = 0. \tag{17}$$

Here the potential $V(a)$ is defined as

$$V(a) = f(a) - \big[2\pi a\sigma(a)\big]^2. \tag{18}$$

Expanding $V(a)$ around a_0, we obtain

$$V(a) = V(a_0) + V'(a_0)(a - a_0) + \frac{1}{2}V''(a_0)(a - a_0)^2 + O\big[(a - a_0)^3\big], \tag{19}$$

where the prime denotes the derivative with respect to a. Since we are linearizing around $a = a_0$, we require that $V(a_0) = 0$ and $V'(a_0) = 0$. The configuration will be in stable equilibrium if $V''(a_0) > 0$. The subsequent analysis will depend on a parameter β, which is usually interpreted as the subluminal speed of sound and is given by the relation

$$\beta^2(\sigma) = \frac{\partial p}{\partial \sigma}\bigg|_\sigma.$$

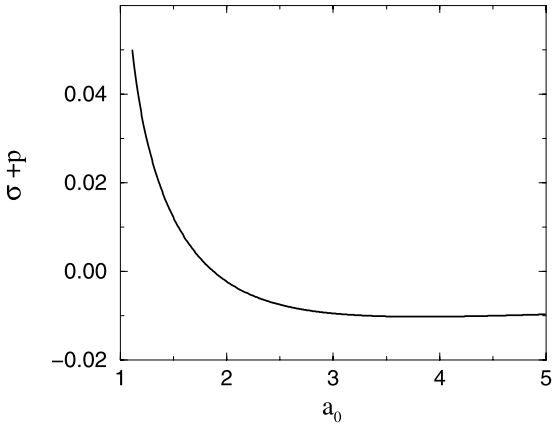

Fig. 15 We plot $y \equiv p + \sigma$ vs. $x \equiv a_0$

To that end, we start with (8) and deduce that $(a\sigma)' = -(\sigma + 2p)$. Also,

$$(a\sigma)'' = -(\sigma' + 2p') = -\sigma'\left(1 + 2\frac{\partial p}{\partial \sigma}\right)$$
$$= 2\left(1 + 2\frac{\partial p}{\partial \sigma}\right)\frac{\sigma + p}{a} = 2(1 + 2\beta^2)\frac{\sigma + p}{a}.$$

Returning to (18), we now obtain

$$V'(a) = f'(a) + 8\pi^2 a\sigma(\sigma + 2p)$$

and

$$V''(a) = f''(a) - 8\pi^2(\sigma + 2p)^2 - 8\pi^2\big[2\sigma(1 + \beta^2)(\sigma + p)\big].$$

When evaluating at the static solution $a = a_0$, we get the expected results $V(a_0) = 0$ and $V'(a_0) = 0$. The stability condition $V''(a_0) > 0$ now yields the intermediate result

$$2\sigma(\sigma + p)(1 + 2\beta^2) < \frac{f''(a_0)}{8\pi^2} - (\sigma + 2p)^2. \tag{20}$$

Recall that σ is negative. If $\sigma + p$ is also negative, then we retain the sense of the inequality to get

$$\beta^2 < \frac{\frac{f''(a_0)}{8\pi^2} - (\sigma + 2p)^2 - 2\sigma(\sigma + p)}{2[2\sigma(\sigma + p)]}; \tag{21}$$

and whenever $\sigma + p > 0$, we have

$$\beta^2 > \frac{\frac{f''(a_0)}{8\pi^2} - (\sigma + 2p)^2 - 2\sigma(\sigma + p)}{2[2\sigma(\sigma + p)]}. \tag{22}$$

The graph of $\sigma + p$ is shown in Fig. 15.

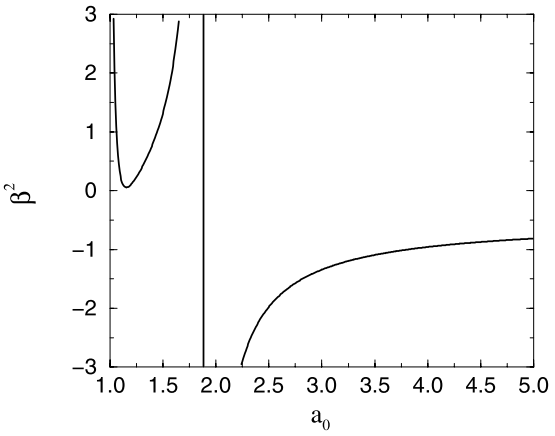

Fig. 16 We plot $y \equiv \beta^2$ vs. $x \equiv a_0$. The region of stability is above the curve on the left and below the curve on the right

There is a region of stability corresponding to $\beta^2 < 1$ provided that Q is close to $1.05M$. (Recall from Sect. 1 that $|Q| < 1.05M$ whenever there are two event horizons.) Figure 16 shows a typical region of stability by choosing $M = 1$ and $Q = 1.049$. To show how close Q has to be to the upper bound, if we let $M = 1$ and $Q = 1.036$, for example, then the region of stability barely reaches down to $\beta^2 = 1$.

For ordinary matter, β represents the velocity of sound since $\beta^2 = \partial p/\partial\rho$ is the square of the rate of change of distance with respect to time. Since we are dealing with exotic matter, this interpretation of β can be questioned. (See Ref. [2] for a discussion.) We take the conservative approach and assume that $0 < \beta^2 \leq 1$, thereby ensuring that there is indeed a region of stability. For the choices of Q and M in Fig. 16, this requirement is met for $a_0 \in [1.06, 1.46]$, approximately. The result makes an interesting contrast to the wormhole in Ref. [2], constructed by using two copies of Schwarzschild spacetime. For that wormhole there are two separate regions of stability that do not include the values $0 < \beta^2 \leq 1$, i.e., the wormhole is unstable for all values of a_0 whenever β is in this range.

7 Conclusion

This paper investigates a new thin-shell wormhole constructed by applying the cut-and-paste technique to two regular charged black-hole spacetimes first introduced by Ayon-Beato and García. The construction allows a graphical description of both σ and p as functions of the radius a of the thin shell, using various values of the mass M and the charge Q. The same parameters help determine whether the wormhole is attractive or repulsive. Finally, the total amount of exotic matter required is determined both analytically and graphically.

The issue of stability to linearized radial perturbations is addressed with the help of the parameter β^2. This yields a region of stability for $\beta^2 \leq 1$ provided that $|Q|$ is less than but close to $1.05M$.

For our wormhole, the parameter β, which is normally interpreted as the speed of sound, has the desired values $0 < \beta^2 \leq 1$ in the region of stability, unlike the wormholes constructed from two Schwarzschild spacetimes [2]. These are unstable for all values of $a = a_0$ whenever $0 < \beta^2 \leq 1$.

References

1. Visser, M.: Nucl. Phys. B **328**, 203 (1989)
2. Poisson, E., Visser, M.: Phys. Rev. D **52**, 7318 (1995)
3. Lobo, F.S.N., Crawford, P.: Class. Quantum Gravity **21**, 391 (2004)
4. Lobo, F.S.N.: Class. Quantum Gravity **21**, 4811 (2004)
5. Eiroa, E.F., Romero, G.: Gen. Relativ. Gravit. **36**, 651 (2004)
6. Eiroa, E.F., Simeone, C.: Phys. Rev. D **70**, 044008 (2004)
7. Eiroa, E.F., Simeone, C.: Phys. Rev. D **71**, 127501 (2005)
8. Thibeault, M., Simeone, C., Eiroa, E.F.: Gen. Relativ. Gravit. **38**, 1593 (2006)
9. Lobo, F.S.N.: Phys. Rev. D **71**, 124022 (2005)
10. Rahaman, F., et al.: Gen. Relativ. Gravit. **38**, 1687 (2006)
11. Eiroa, E.F., Simeone, C.: Phys. Rev. D **76**, 024021 (2007)
12. Rahaman, F., et al.: Int. J. Mod. Phys. D **16**, 1669 (2007)
13. Rahaman, F., et al.: Gen. Relativ. Gravit. **39**, 945 (2007)
14. Rahaman, F., et al.: Chin. J. Phys. **45**, 518 (2007). arXiv:0705.0740 [gr-qc]
15. Richarte, M.G., Simeone, C.: Phys. Rev. D **76**, 087502 (2007)
16. Lemos, J.P.S., Lobo, F.S.N.: Phys. Rev. D **78**, 044030 (2008)
17. Rahaman, F., et al.: Acta Phys. Polon. B **40**, 1575 (2009). arXiv:0804.3852 [gr-qc]
18. Rahaman, F., et al.: Mod. Phys. Lett. A **24**, 53 (2009). arXiv:0806.1391 [gr-qc]
19. Eiroa, E.F.: Phys. Rev. D **78**, 024018 (2008)
20. Eiroa, E.F., Richarte, M.G., Simeone, C.: Phys. Lett. A **373**, 1 (2008)
21. Ayon-Beato, E., García, A.: Phys. Lett. B **464**, 25 (1999)
22. Roman, T.A.: Phys. Rev. D **53**, 5496 (1993)